# Combination of Correlated Phase Error Correction and Sparsity Models for SAR

Toby Sanders[a] and Theresa Scarnati[b]

[a,b]School of Math & Stat Sciences, Arizona State University, Tempe, AZ

## ABSTRACT

Direct image formation in synthetic aperture radar (SAR) involves processing of data modeled as Fourier coefficients that lie on a polar grid. Often in such data acquisition processes, imperfections in the data cannot simply be modeled as additive or even multiplicative noise errors. In the case of SAR, errors in the data can exist due to the imprecise estimation of the round trip wave propagation time, which manifests as linearly varying phase errors in the antenna data across the pulses. To correct for these errors, we propose a phase correction scheme that relies on both the on smoothness characteristics of the image and the phase corrections associated with neighboring pulses, which are possibly highly correlated due to the nature of the data offsetting. Our model takes advantage of these correlations and smoothness characteristics simultaneously for a new autofocusing approach. Our algorithm for the proposed model alternates between approximation of image features and phase error estimates according to the model.

**Keywords:** synthetic aperture radar, $\ell_1$ regularization, phase errors, autofocusing

## 1. INTRODUCTION

Imaging via synthetic aperture radar (SAR) is a well-established technique for effective scene imaging under most conditions, with resolution up to a few centimeters.[1,2] SAR works by acquiring data from a number of different viewpoints, or azimuth angles, by moving the transmission mechanism around a flight path about the scene. At each azimuth angle, an electromagnetic (EM) wave with microwave length frequencies is transmitted towards the scene and scattered from obstructions, or "scatterers," within the scene. The scattered echo response from the scene is measured, and it serves as the data from which to reconstruct the image.

This measurement process requires knowledge of the round trip time required for the EM wave to travel to the scene and return back to the sensing mechanism. Under ideal conditions, the distance from the scene center to the transmission and sensing mechanisms is accurately known, and the EM wave travels at precisely the speed to light in a vacuum. In this setting, the round trip time is assumed to be known perfectly. In practice however, this distance may only be approximately known, and atmospheric disturbances can delay the wave propagation. Moreover, because EM waves propagate at a very high speed, minute errors in the measurement of the distance to the scene can result in significant relative errors in the round trip time estimates. These errors manifest as phase errors in a reconstructed image, which is then characterized as *defocused*. Thus, a number of autofocusing algorithms have been designed to alleviate this issue.[3–6]

Typically, the Phase Gradient Autofocus (PGA) algorithm[5,7] has been used to correct for these errors. PGA is an iterative post processing algorithm that makes a robust estimation of the gradient of the phase error. The estimation process exploits the redundancy of the phase error information contained in the defocused image. The PGA algorithm requires circular shifting of data to remove frequency offset due to Doppler shifting of the scatterer, windowing of the circularly shifted imagery to preserve the width of the dominant scatterers in the scene, a phase gradient estimation, and an iterative correction process to remove any estimation bias.

Within the PGA algorithm, Fourier transforms between the image and the range-compressed domains are required for each iteration, and such processing must be performed over many range bins to take advantage of

Further author information:
T.L.S.: E-mail: tlsander@asu.edu
T.A.S.: E-mail: tscarnat@asu.edu

Computational Imaging II, edited by A. Mahalanobis, A. Ashok, L. Tian, J. C. Petruccelli, K. S. Kubala,
Proc. of SPIE Vol. 10222, 102220E · © 2017 SPIE · CCC code: 0277-786X/17/$18 · doi: 10.1117/12.2262861

the redundancy in the data. Thus, the PGA algorithm can become computationally burdensome. Also, PGA is strictly a post processing algorithm.

Alternatively, we propose a regularization based autofocusing procedure that jointly estimates the underlying image and its corresponding phase errors. Similar techniques were proposed in Ref. 3,8–10, however our algorithm additionally exploits the redundancies and correlations present in the unknown phase errors. In addition, we more carefully exploit the nature of the unknown phase errors, as they vary linearly with respect to the frequencies.

In Ref. 10, a weighted least-squares estimation of these phase errors is formulated without making assumptions on the noise model or underlying scene. The weights are calculated to be inversely proportional to the variance of the phase in each range bin, and the method is shown to minimize the variance of the residual phase error. Though this method is robust to various noise models, estimation can be improved by the incorporation of prior knowledge about the scene and phase errors.

The effects of phase errors on an under-sampled SAR system were investigated by Kelly et. al. in Ref. 8. The authors consider the SAR data to be under-sampled in the cross-range dimension, with phase errors assumed constant. They assume a sparse number of scatterers in the underlying scene and jointly optimize for the phase errors and the imagery. Uur and Arıkan[9] improve the the work of Kelley et. al.[8] by incorporating a total variation constraint on the reconstructed scene.

Related approaches to this paper were demonstrated in Ref. 3 and Ref. 11. The authors enforce that the phase errors vary along the cross-range direction in the frequency domain. The phase errors and imagery are found through an alternating optimization procedure, and the underlying scene is assumed to be dominated by a small number of strong scatterers. This assumption on the scene was incorporated into the cost function by sparsity promoting $\ell_1$ and $\ell_p$ norms with $p < 1$. Though the results are promising, these previous papers do not model the true correlation of phase errors across azimuth locations, and do not exploit the linearly varying phase error with respect to the frequencies. In the development of our techniques, we will exploit these correlations through additional regularization constraints, while also enforcing smoothness and sharpness of edges within the scene.

## 2. PROBLEM DESCRIPTION

In the following development of the problem, we generally follow the work of Jakowatz et. al.,[12] in particular the content contained within Chapter 4. We let $f$ denote be the 2D reflective scene of scattering objects that we want to image, and suppose $f$ is defined over a disc centered at the origin with radius $R_0$. Then at a particular position in the sensing process, indicated by an azimuth angle $\theta$, the transmitted linear FM chirp mixes with the scene in a way which is dependent upon the angle $\theta$ that the chirp is emitted*. In particular, in the far field case, once the transmitted signal reaches the scene it has essentially a planar wave front, and thus the points in the scene along each line perpendicular to the direction of the chirp all mix with the same values. Therefore, we can simplify this 2D setup to a 1D process by compressing the scatterers along each of these lines to a single point. We call this compression the projection of $f$ or, more generally, the Radon transform of $f$ at angle $\theta$, which can be expressed mathematically as

$$Pf(u,\theta) = \iint\limits_{x^2+y^2\leq R_0^2} f(x,y)\delta(u-(x,y)\cdot(\cos\theta,\sin\theta))\,dx\,dy \tag{1}$$

The microwave signal that is transmitted and mixes with the scene is given by the real part of

$$s(t) = \begin{cases} e^{i(\omega t+\alpha t^2)}, & |t|\leq \frac{T}{2} \\ 0, & \text{otherwise} \end{cases}, \tag{2}$$

where $\omega$ is the carrier frequency, $2\alpha$ is the chirp rate, and $T > 0$ is the pulse duration. This chirp signal mixes with the scene to yield reflected signals of the form

$$r(t,\theta) = \mathbf{Re}\Big\{\int_{-R_0}^{R_0} Pf(u,\theta)(s(t-\tau_0-\tau(u)))\,du\Big\}. \tag{3}$$

*In practice, there is also a relevant angle of elevation, but we can ignore it here.

Here $\tau_0 + \tau(u)$ is the *estimated* round trip time for the chirp to travel to the scene position $u$. The value $\tau_0$ is the round trip time required for the chirp to travel to the scene center, and $\tau(u)$ is the additional travel time for any particular position in the scene $u$. These values are given by $\tau_0 = 2R/c$ and $\tau(u) = 2u/c$, where $R$ is the distance from the transmitter/receiver to the scene center, and $c$ is the speed of light in a vacuum.

In order to *extract* approximate instantaneous frequency information (i.e. the classical Fourier transform of $f$) from the chirp response, a *deramping* process is implemented. In brief, this process requires the following steps:

1. Demodulation of $r(t,\theta)$ for each $\theta$ by multiplication with

$$d_1(t) = \cos(\omega(t-\tau_0) + \alpha(t-\tau_0)^2) \quad \text{and} \quad d_2(t) = \sin(\omega(t-\tau_0) + \alpha(t-\tau_0)^2) \tag{4}$$

   to obtain $r_d(t,\theta) = r(t,\theta)(d_1(t) - id_2(t))$. Using the appropriate trigonometric identities, one can show this yields

$$\begin{aligned} r_d(t,\theta) = \frac{1}{2}\int_{-R_0}^{R_0} Pf(u,\theta)\exp\{i(w(2t-\tau(u)-2\tau_0) \\ + \alpha((t-\tau_0)^2 + (t-\tau(u)-\tau_0)^2))\}\,du \\ + \frac{1}{2}\int_{-R_0}^{R_0} Pf(u,\theta)\exp\{i(\alpha\tau^2(u) - \tau(u)(\omega + 2\alpha(t-\tau_0)))\}\,du. \end{aligned} \tag{5}$$

2. Low pass filtering of the result from step 1 to remove the first term.

From here, if we suppose that the chirp rate $\alpha$ and the scene radius $R_0$ are sufficiently small, then $\alpha\tau^2(u) = \frac{4\alpha u^2}{c^2} \approx 0$, so that $e^{\alpha\tau^2(u)} \approx 1$, then the resulting approximation is given by

$$r_{\ell,d}(k,\theta) = \int_{-R_0}^{R_0} Pf(u,\theta)e^{-iku}\,du, \tag{6}$$

where $k = k(t) := \frac{2}{c}(\omega + 2\alpha(t-\tau_0))$. In other words, the demodulation approximately yields the Fourier coefficients of the projection of $f$, which are just Fourier coefficients of $f$ by the projection slice theorem, i.e. $r_{\ell,d}(k,\theta) = \hat{f}(k\cos\theta, k\sin\theta)$ where $\hat{f}$ denotes the Fourier transform of $f$.

An error in the estimated round trip propagation time means that the input $\tau_0$ is incorrect, which likely varies with respect to the particular angle. Therefore, to determine the result of this error, we may replace $\tau_0$ by $\tau_0 + \epsilon(\theta)$ in either (3) or (4). Doing so, and again performing the same calculations as were done in the case of no error, yields

$$\tilde{r}_{\ell,d}(k,\theta) = e^{-ik\phi(\theta)}\int_{-R_0}^{R_0} Pf(u,\theta)e^{-iku}\,du, \tag{7}$$

where $\phi(\theta) = \frac{\epsilon(\theta)c}{2}$ and $k$ is as before. Here, we also used the approximation $\alpha\epsilon^2(\theta) \approx 0$.

## 3. PROPOSED AUTOFOCUSING

Our proposed autofocusing algorithm follows the general methodology proposed by Cetin et. al. and others,[3,6,11] by alternating between the recovery of the image information $f$ and the phase errors $\phi(\theta)$. The significant alternative to our approach is in the characterization of the phase errors as varying linearly as written in (7).

For the necessary discretization of the problem, suppose the frequencies values are given by $k_1, k_2, \ldots, k_N$, and the angles are given by $\theta_1, \theta_2, \ldots, \theta_P$, where the indexing of each is by increasing order. Let $\mathcal{F} : C^{n\times n} \to C^{N\cdot P}$ denote the ideal forward operator that maps $f \in C^{n\times n}$ to $r_{\ell,d}(k,\theta)$ as given in (6).[†] Let $b$ denote the vector containing the ideal data given by $b = \{r_{\ell,d}(k_i,\theta_j)\}_{i,j=1}^{N,P}$, and let $\tilde{b}$ denote the data vector containing phase errors

[†]Here we're now assuming a discretization of the continuous integral by pixelation of $f$.

given by $\tilde{b} = \{\tilde{r}_{\ell,d}(k_i, \theta_j)\}_{i,j=1}^{N,P}$. Then, the classical problem is to find $f$ satisfying $\mathcal{F}f = b$, yet in practice we are solving $\mathcal{F}f = \tilde{b}$. Thus, letting our vector of phase errors be denoted by $\vec{\phi} = \{\phi(\theta_j)\}_{j=1}^{P}$, we may correct for these errors by building a *correction* to the forward model given by

$$E = E(\vec{\phi}) = \text{diag}\{e^{-ik_i\phi(\theta_j)}\}_{i,j=1}^{N,P}. \tag{8}$$

With $\vec{\phi}$ known we have an accurate forward model. However, these values are unknown in practice, and we must design our algorithm to attempt to recover these values along with the image. Because the platform position uncertainties will remain constant over a signal received at one location $\theta$ but will vary across locations $\theta_j$ for $j = 1, ...P$, the phase errors are constant across frequencies and only vary along the azimuth direction. Also, the platform does not vary immensely from one aperture to the next. Thus, perhaps the phase errors $\phi(\theta_j)$ are correlated in the sense that the errors at nearby locations are similar, i.e., $\nabla\vec{\phi}$ is relatively small. This information is used as an additional tool to recover these errors.

We incorporate the recovery of $\vec{\phi}$ and $f$ with the popular $\ell_1$ regularization techniques, that also makes use of the a priori knowledge of the sparsity of $f$ in a smoothness domain. For example, TV regularization is often used, which assumes a sparse number of boundaries or edges within the image. For SAR, this model must be modestly adapted due to the observation of random phases in the complex image, regardless of the image reconstruction approach.

Our $\ell_1$ regularization model then is

$$\min_{f,\phi} \left\{ \frac{\lambda}{2}\|E(\phi)\mathcal{F}f - \tilde{b}\|_2^2 + \|Tf\|_1 + \frac{\zeta}{2}\|\nabla\phi\|_2^2 + \frac{\kappa}{2}\|\phi\|_2^2 \right\}. \tag{9}$$

Here $T$ is the transform from which the image is assumed to be sparse, and in the case of TV regularization is a first order finite difference operator. Again, this must be modestly adapted for SAR to account for random phase values of the pixels.[13] Regularization of $\phi$ is encouraged through the $\ell_2$ norm of the gradient, as we assume small variations in the errors, but not necessarily sparsity in these variations, which the $\ell_1$ norm would encourage.

To numerically solve this problem, we propose alternating minimization over $f$ and $\phi$. The minimization over $f$ is a nontrivial, yet well-document problem. In particular it may be solved efficiently by introducing a splitting variable, which allows one to solve equivalent subproblems.[14,15]

However, in our setup minimization over $\phi$ is not common practice. The main concern is the introduction of the exponential term $E(\phi)$ within the quadratic penalty. Nevertheless, we derive an appropriate gradient decent algorithm to perform this minimization.

### 3.1 Minimization Over $\phi$

At some iteration $n$, given current solutions $f^n$ and $\phi^n$, suppose we would like to find $\phi^{n+1}$ by gradient decent. Then we need to compute the gradient of the functional

$$H(\phi; f) = \frac{\lambda}{2}\|E(\phi)\mathcal{F}f - \tilde{b}\|_2^2 + \frac{\zeta}{2}\|\nabla\phi\|_2^2 + \frac{\kappa}{2}\|\phi\|_2^2 \tag{10}$$

with respect to $\phi$ evaluated at the current solutions. The gradient of the latter two terms with respect to $\phi$ is

$$\zeta\nabla^T\nabla\phi + \kappa\phi. \tag{11}$$

To determine the gradient of $\|E(\phi)\mathcal{F}f - \tilde{b}\|_2^2$, first let $x := \mathcal{F}f$. Moreover, re-index $x$ and $\tilde{b}$ be by frequency and pulse, i.e. $\tilde{b} = \{\tilde{b}_{\ell,j}\}_{\ell,j=1}^{N,P}$ and similarly for $x$. Then this norm can be expanded as

$$\|E(\phi)\mathcal{F}f - \tilde{b}\|_2^2 = \sum_{j=1}^{P}\sum_{\ell=1}^{N} |e^{-i\phi_j k_\ell}x_{\ell,j} - \tilde{b}_{\ell,j}|^2 \tag{12}$$

To compute the partial derivatives of the expression with respect to $\phi_j$, we first observe that in general for $a, b \in \mathbb{C}$ and $\phi, k \in \mathbb{R}$ we have

$$\frac{\partial}{\partial \phi}\left(|ae^{i\phi k} - b|^2\right) = \mathbf{Re}\left(-2ika\bar{b}e^{ik\phi}\right) \tag{13}$$

Combining Equation (12) and Equation (13) leads to

$$\frac{\partial}{\partial \phi_j}\left(\|E(\phi)\mathcal{F}f - \tilde{b}\|_2^2\right) = 2\mathbf{Re}\left\{\sum_{\ell=1}^{N} ik_\ell x_{\ell,j}\overline{\tilde{b}_{\ell,j}}e^{-i\phi_j k_\ell}\right\} \tag{14}$$

Assuming that $x = \mathcal{F}f$ is predetermined, this expression is numerically inexpensive to compute via Hadamard products. To show this, let $\odot$ denote the Hadamard product of two vectors, $\mathbf{k} = \{k_\ell\}_{\ell=1}^N$, $\mathbf{b}_j = \{\tilde{b}_{\ell,j}\}_{\ell=1}^N$, and $E(\phi_j)$ denote the entries of $E(\phi)$ only involving $\phi_j$. Then using (14) it can be shown that the gradient with respect to $\phi$ is given by

$$\nabla_\phi \|E(\phi)\mathcal{F}f - \tilde{b}\|_2^2 = \{2\mathbf{Re}\langle i\mathbf{k} \odot (E(\phi_j)x), \mathbf{b}_j\rangle\}_{j=1}^P \tag{15}$$

Finally, evaluating at the current iterates $f^n$ and $\phi^n$, multiplication by $\lambda/2$, and combining with Equation (11) completes the expression for the necessary gradient of $H$ with respect to $\phi$:

$$\nabla_\phi H(\phi^n, f) = \lambda\{\mathbf{Re}\langle i\mathbf{k} \odot (E(\phi_j^n)x), \mathbf{b}_j\rangle\}_{j=1}^P + \zeta\nabla^T\nabla\phi^n + \kappa\phi^n \tag{16}$$

Then, each update over $\phi$ takes the form

$$\phi^{n+1} = \phi^n - \alpha\nabla_\phi H(\phi^n; f), \tag{17}$$

where the appropriate step length $\alpha$ is determined via backtracking.[16]

## 4. NUMERICAL ALGORITHM

We first formulate an equivalent alternative to (9) by introduction a splitting variable $g$:

$$\min_{f,g,\phi}\left\{\frac{\lambda}{2}\|E(\phi)\mathcal{F}f - \tilde{b}\|_2^2 + \|g\|_1 + \frac{\zeta}{2}\|\nabla\phi\|_2^2 + \frac{\kappa}{2}\|\phi\|_2^2 \quad \text{s.t.} \quad Tf = g\right\}. \tag{18}$$

To approximate this constrained optimization problem, we solve

$$\begin{aligned}\min_{f,g,\phi} J_\sigma(f, g; \phi) = \min_{f,g,\phi}\Big\{&\frac{\lambda}{2}\|E(\phi)\mathcal{F}f - \tilde{b}\|_2^2 + \|g\|_1 + \frac{\zeta}{2}\|\nabla\phi\|_2^2 + \frac{\kappa}{2}\|\phi\|_2^2 \\ &+ \frac{\beta}{2}\|Tf - g\|_2^2 - \langle\sigma, Tf - g\rangle\Big\}.\end{aligned} \tag{19}$$

The new terms enforce the constrained terms, and in particular if the Lagrangian multiplier $\sigma$ is updated a sufficient number of times then we suitably approximate the constrained problem. Setting the $\phi$ terms aside, our numerical algorithm for the $\ell_1$ optimization generally follows the popular alternating minimization algorithm implemented Li and others.[14] Our $\ell_1$ optimization algorithm is available online.[17]

The minimization of this functional is approximated by iterative alternating minimization over $f, g$, and $\phi$, while making updates on the Lagrange multiplier $\sigma$. Our alternating minimization is designed for stability and accuracy. One could simply select alternating one by one over updates on $f$, $g$, $\phi$, and $\sigma$, but this is likely would produce suboptimal results. In particular, updates on $\sigma$ and $\phi$ fundamentally change the objective functional as a function of $f$. Because updates on $f$ are computed by gradient decent, we must "restart" the gradient decent procedure whenever $\phi$ or $\sigma$ are updated.

To this end, after an initialization of the variables, the algorithm alternates between updates on $f$ and $g$. Once these variables have been updated a suitable number of times (e.g. 10 or 15), the algorithm then performs

a minimization procedure over $\phi$ using several gradient decent iterations. The gradient descent iterations are not computationally burdensome. Finally, the Lagrangian multiplier is updated according the standard formula

$$\sigma^{new} = \sigma^{old} - \beta(Tf - g), \tag{20}$$

using the current values of $f$ and $g$.

The gradient decent over $\phi$ was detailed in Section 3.1. For minimization over $g$, given current values of $f$ and $\sigma$, the exact minimum is given by

$$g^{new} = \max\left(\left|Tf - \frac{\sigma}{\beta}\right| - \frac{1}{\beta}, 0\right) * sign\left(Tf - \frac{\sigma}{\beta}\right). \tag{21}$$

Updates over $f$ take the form

$$f^{new} = f^{old} - \alpha\nabla_f J_\sigma, \tag{22}$$

where the gradient of $J_\sigma$ with respect to $f$ is given by

$$\nabla_f J_\sigma = \lambda\mathcal{F}^*\mathcal{F}f - \mathcal{F}^*E(\overline{\phi})\tilde{b} + \beta T^*(Tf - g) - T^*\sigma \tag{23}$$

A pseudo algorithm outlining this numerical scheme is given below.

**Algorithm 1**

Determine parameters for the algorithm, and initialize $f$, $g$ and perform a first estimate for $\phi$:
**for** $i = 0$ **to** K **do**
  **while** $\|\phi^{new} - \phi^{old}\| > tol$ **do**
    Update $\phi$ according to (17).
  **end while**
  **while** $\|f^{new} - f^{old}\| > tol$ **do**
    Update $f$ according to (22) and (23).
    Minimize $g$ according to (21).
  **end while**
  Update Lagrange multiplier according to (20).
**end for**

## 5. NUMERICAL RESULTS

We first test our proposed method for minimization over only the $\phi$ subproblem. That is, we assure that we can find the minimum to $H(\phi; f)$ in (10) for some fixed $\mathcal{F}f$ and corresponding fixed phase corrupted data, $\tilde{b} = E(\phi_{true})\mathcal{F}f$. Here $\phi_{true}$ are the true correlated phase errors with $E(\phi_{true})$ as in (8).

The results for this minimization in 4 simulations is shown in Figure 1. Here we have plotted the true, generated phase errors against the errors recovered by our algorithm. The results in the top row indicate relatively small estimation errors, and our algorithm successfully recovered almost all phase values. However, in the bottom row, where we have relatively larger phase errors, it appears we have only successfully recovered about half of the values. The errors which are incorrect appear to be all off by precisely two units.

The reason for these two unit jumps is the well-known phase wrapping problem, or rather phase *unwrapping*. To explain it simply, let $k \in \mathbb{R}$. Then obviously $e^{ik} = e^{i(k+2\pi)}$, hence for values of $k \notin (-\pi, \pi]$ we recover the wrapped phase within $(-\pi, \pi]$ instead of the true unwrapped phase. Therefore for the larger phase errors shown in Figure 1 we are recovering the wrapped phase. In general, recovery of the wrapped phase will not provide the proper data corrections necessary for autofocusing. Although this sort of issue is well-known for these types of problems,[18,19] it was unforeseen by the authors and has proven to be a worthy obstacle for future work. To this end, we test our full image recovery algorithm for cases when errors are sufficiently small to avoid any phase wrapping. Unfortunately, this means that the defocusing due to the introduction of the phase errors is limited.

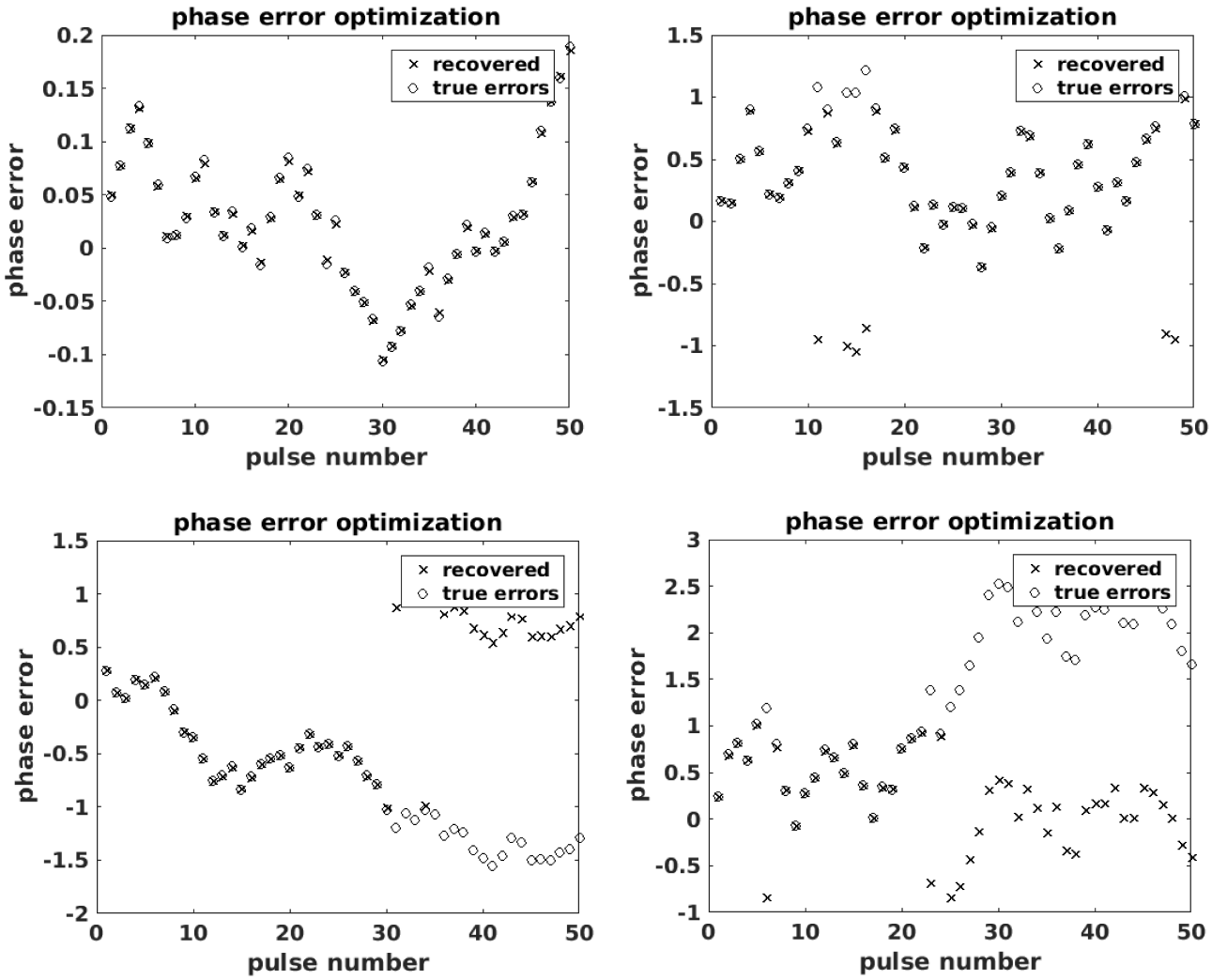


Figure 1. Simulations for minimization procedure over only the phase errors, $\phi$. Larger phase errors show the infamous phase wrapping problem.

We simulate the phase errors by the first computing the polar Fourier coefficients of the test images, and then multiplying by generated phase errors. The Fourier coefficients are calculated using the accurate non-uniform FFT (NUFFT) developed by Fessler and Sutton.[20] Then the small correlated phase errors are generated in a sequential fashion. In particular, each phase errors is randomly selected from a normal distribution with a mean set to 0.9 times the previous phase error. This results in correlated phase errors that trend back to zero.

We used two 200×200 simple test images, one with larger features and one with 3 small circular targets. In each case, the error free data take the form of

$$r_{\ell,d}(k,\theta) \approx \hat{f}_{k,\theta} = \sum_{m,n=0}^{N-1} f_{m,n} e^{-ik(\cos\theta,\sin\theta)\cdot(m,n)}. \tag{24}$$

The frequency values $k$ here are discretized values over the interval $[-\pi, 3\pi]$. If we assume each pixel is $1.5\text{cm}^2$, then the corresponding central frequency is approximately 10 GHz. The regularization parameters are chosen such that $\lambda = 200$, $\beta = 30$, $\kappa = 0.05$ and $\zeta = 0.2$, with the default normalizations built into the original algorithm.[17]

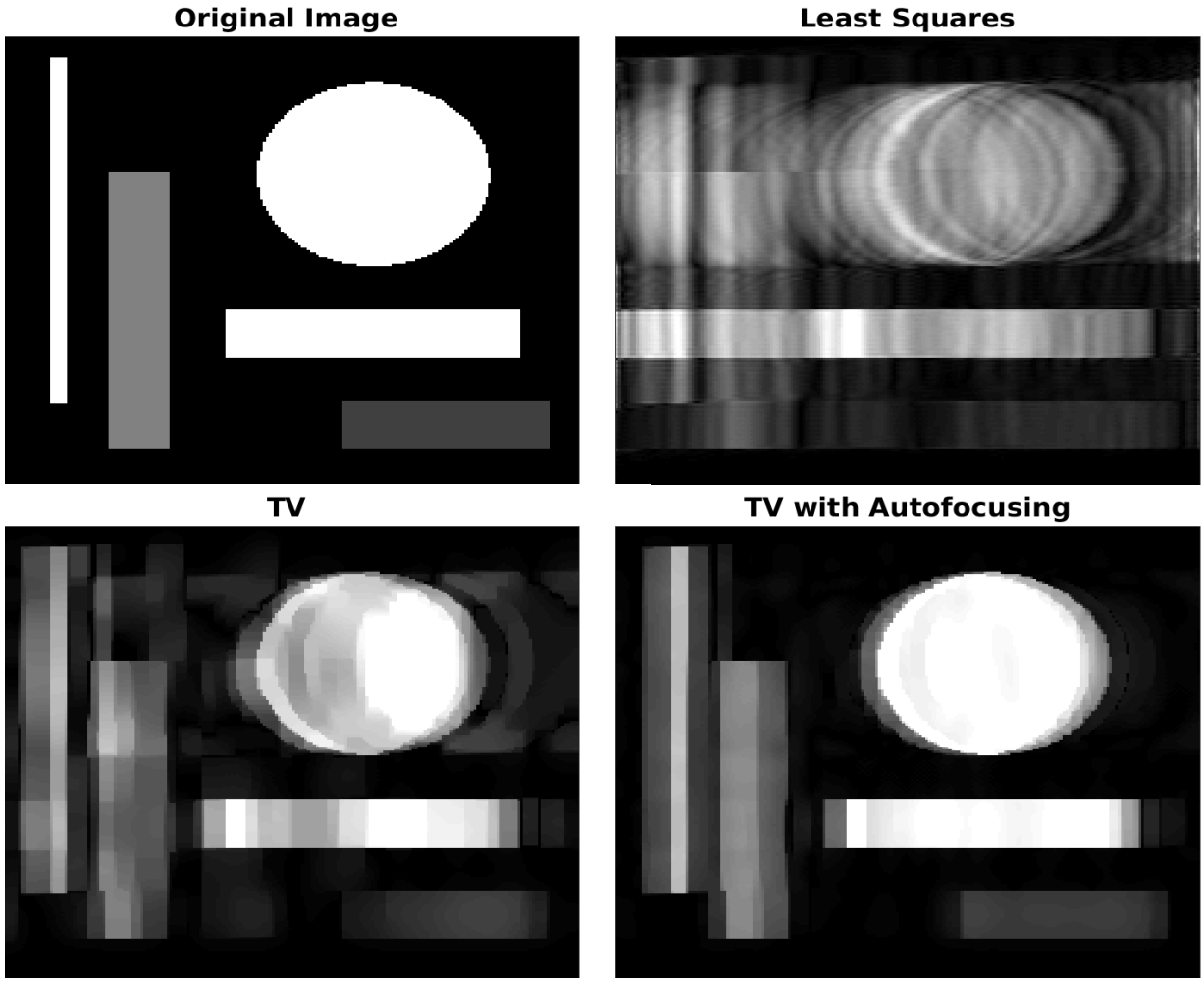


Figure 2. Results for SAR reconstructions from defocused data.

The results for the first test image are shown in Figure 2, where a 10° aperture was used. There is a clear defocusing effect in the TV (bottom left) and least squares solution (top right). However, the TV regularization did remove some of the effects. The results from our dual TV and phase estimation algorithm (bottom right) indicates significant improvement, although some small defocusing effects are still present. The results for second test image are shown in Figure 3, where, in this case, we used a 60° aperture. In this example, there is again notable defocusing effects in the TV and least squares solutions. For this simulation however, the TV does not indicate any improvement over the least squares. On the other hand, our proposed algorithm yields near perfect reconstruction.

Finally, as a quantitative result, we ran 100 defocusing simulations on the Shepp-Logan phantom with a 10° aperture. Here we are interested in how well each algorithm fits the data corrupted with the phase error compared with the exact data, which is unknown to the algorithm. In other words, if $f$ is the reconstructed image, $b$ is the exact data, and $\tilde{b}$ is the input phase corrupted data, then we are interested in comparing $\|\mathcal{F}f - b\|_2$ and $\|\mathcal{F}f - \tilde{b}\|_2$. Certainly we expect the latter error measure to be smaller without any autofocusing, but a good reconstruction would have the former error to be smaller. Indeed, shown in Figure 4 are the results from these 100 simulations, and the least squares and TV reconstructions both satisfy $\|\mathcal{F}f - b\|_2 > \|\mathcal{F}f - \tilde{b}\|_2$ in essentially all cases. However, the TV does show some modest improvements to least squares in this regard. As a very promising result, our autofocusing approach satisfies the opposite inequality in what appears to be all but a few simulations.

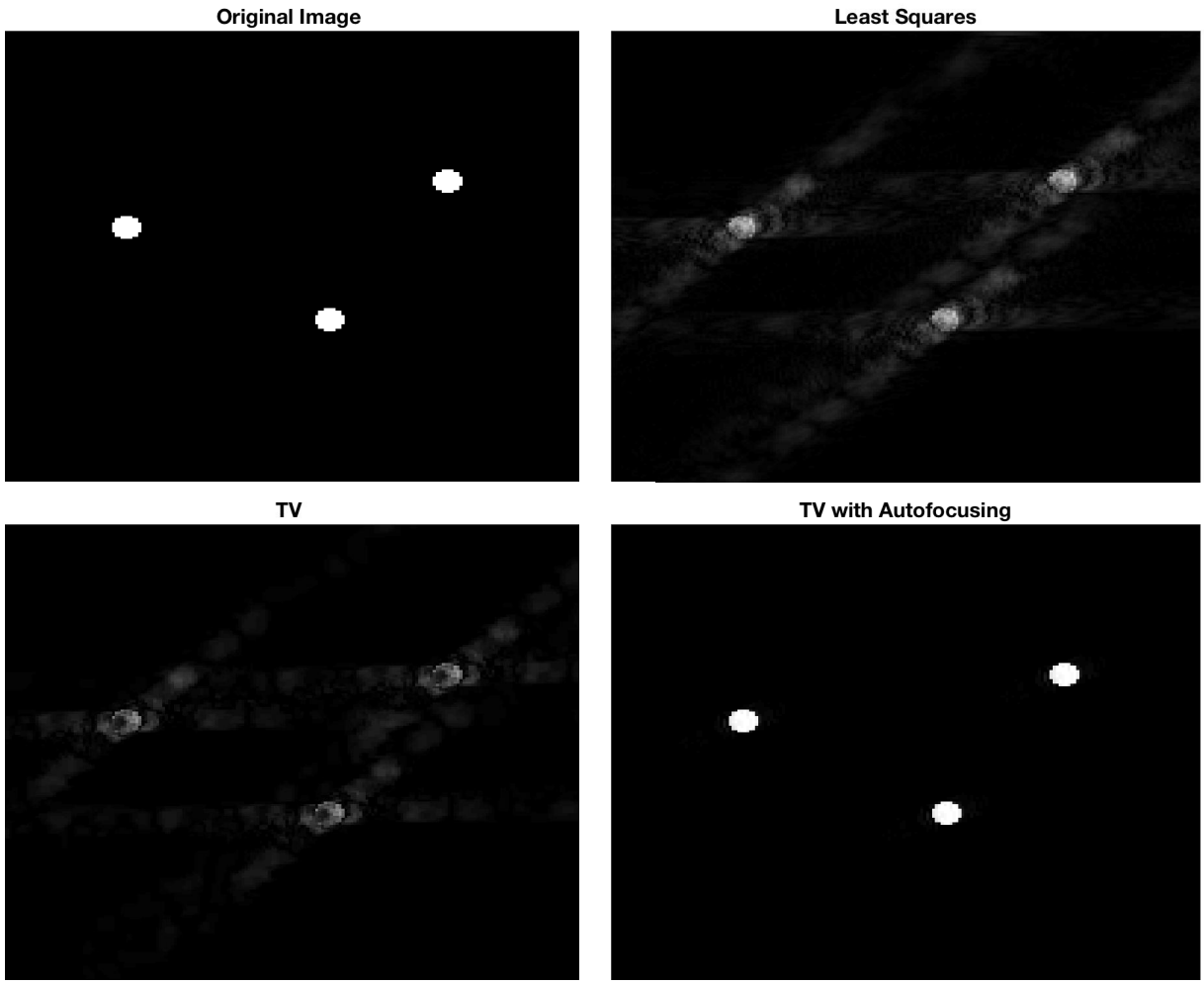


Figure 3. Results for SAR reconstructions from defocused data.

## 6. SUMMARY

In this investigation we developed a new autofocusing technique for SAR image formation. Specifically, we propose an iterative optimization algorithm that jointly estimates SAR imagery while correcting for phase errors present in the data. Our algorithm differs significantly from previous approaches due to the result of the derivation of the phase errors manifesting in the data having a linear dependency on the frequencies. Through the inclusion of an TV regularization operator, we incorporate prior knowledge about the sparsity of edges in the scene into our algorithm. In addition, we also enforce the correlation of the phase errors across azimuth angles using regularization, which was not considered in previous autofocusing algorithms.

We first showed that we can successfully recover the introduced phase errors using gradient decent, so long as the errors are sufficiently small so that we avoid the phase wrapping. Because we have control over the magnitude of the phase errors, we can ensure that no phase unwrapping will be necessary in our algorithm at this time. In the future, we would like to incorporate a phase unwrapping scheme into our algorithm so that we may use our techniques to reconstruct defocused SAR images from real measured data.

In this paper, we reconstruct two images from the compiled data using a least squares algorithm, total variation regularization and our proposed autofocusing algorithm. The result of each experiment demonstrates that our algorithm can yield significant improvement to the defocusing problem, and we are able to produce images that have improved visual quality.

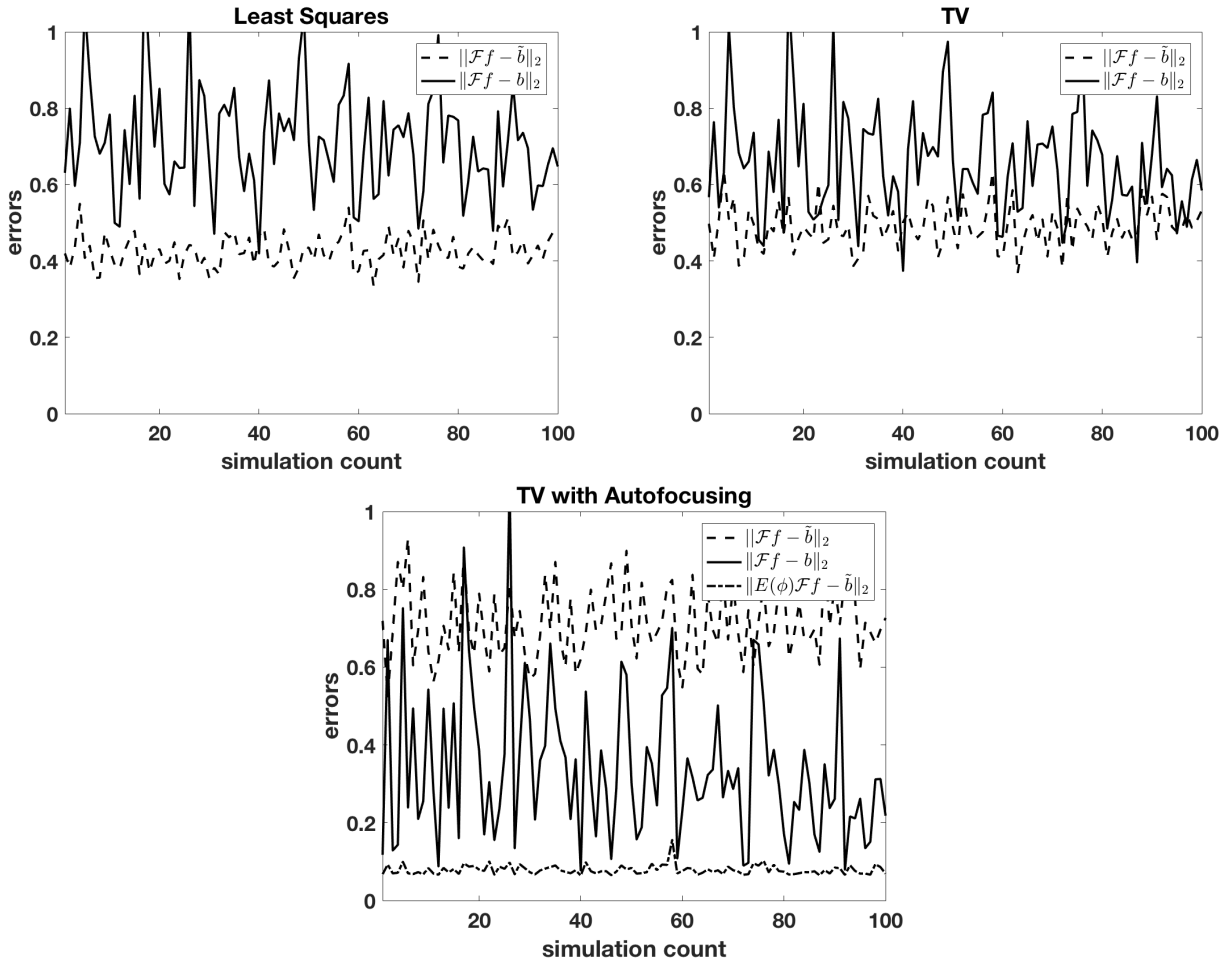


Figure 4. Normalized data fitting errors for each reconstruction over 100 simulations. The data fitting errors are plotted for the input data with phase errors (dashed line) and the exact data (solid line), which was unavailable for the reconstruction. The data fitting with recovered phase errors is also shown in the autofocusing case (dot-dashed line).

To quantitatively verify the improvement that our proposed algorithm produces, we compare how well all algorithms considered fit the data corrupted with the phase error to how well each algorithm fits the exact data. We see that when using typical reconstruction algorithms, the resulting reconstruction more closely fits that of the phase corrupted data. However, with our proposed algorithm, the true data is fitted more accurately, indicating clear improvement.

## ACKNOWLEDGMENTS

This work is supported in part by the grants NSF-DMS 1502640, NSF-DMS 1522639 and AFOSR FA9550-15-1-0152.

## REFERENCES

[1] Natterer, F., Cheney, M., and Borden, B., "Resolution for radar and x-ray tomography," *Inverse Problems* **19**(6), S55 (2003).

[2] Cheney, M. and Borden, B., [*Fundamentals of Radar Imaging*], Society for Industrial and Applied Mathematics (2009).

[3] Onhon, N. Ö. and Cetin, M., "A sparsity-driven approach for joint SAR imaging and phase error correction," *IEEE Transactions on Image Processing* **21**(4), 2075–2088 (2012).

[4] Koo, V. C., Lim, T. S., and Chuah, H. T., "A comparison of autofocus algorithms for SAR imagery," in [*Progress in electromagnetics research symposium*], **1**(1), 16–19 (2005).
[5] Wahl, D. E., Eichel, P., Ghiglia, D., and Jakowatz, C., "Phase gradient autofocus-a robust tool for high resolution SAR phase correction," *IEEE Transactions on Aerospace and Electronic Systems* **30**(3), 827–835 (1994).
[6] Cetin, M., Onhon, O., and Samadi, S., "Handling phase in sparse reconstruction for SAR: Imaging, autofocusing, and moving targets," in [*Synthetic Aperture Radar, 2012. EUSAR. 9th European Conference on*], 207–210, VDE (2012).
[7] Eichel, P., Ghiglia, D., and Jakowatz, C., "Speckle processing method for synthetic-aperture-radar phase correction," *Optics letters* **14**(1), 1–3 (1989).
[8] Kelly, S. I., Yaghoobi, M., and Davies, M. E., "Auto-focus for under-sampled synthetic aperture radar," *Institute for Digital Communications* (2012).
[9] Uur, S. and Arıkan, O., "SAR image reconstruction and autofocus by compressed sensing," *Digital Signal Processing* **22**(6), 923–932 (2012).
[10] Ye, W., Yeo, T. S., and Bao, Z., "Weighted least-squares estimation of phase errors for SAR/ISAR autofocus," *IEEE Transactions on Geoscience and Remote Sensing* **37**(5), 2487–2494 (1999).
[11] Güngör, A., Cetin, M., and Güven, H. E., "An augmented lagrangian method for autofocused compressed sar imaging," in [*Compressed Sensing Theory and its Applications to Radar, Sonar and Remote Sensing (CoSeRa), 2015 3rd International Workshop on*], 1–5, IEEE (2015).
[12] Jakowatz, C. V., Wahl, D. E., Eichel, P. H., Ghiglia, D. C., and Thompson, P. A., [*Spotlight-Mode Synthetic Aperture Radar: A Signal Processing Approach*], Springer Science & Business Media (2012).
[13] Sanders, T., Gelb, A., and Platte, R. B., "Composite sar imaging using sequential joint sparsity," *Journal of Computational Physics* **338**, 357–370 (2017).
[14] Li, C., *An efficient algorithm for total variation regularization with applications to the single pixel camera and compressive sensing*, PhD thesis, Rice University (2009).
[15] Goldstein, T. and Osher, S., "The split Bregman method for l1-regularized problems," *SIAM Journal on Imaging Sciences* **2**(2), 323–343 (2009).
[16] Wright, S. and Nocedal, J., "Numerical optimization," *Springer Science* **35**, 67–68 (1999).
[17] Sanders, T., "Matlab imaging algorithms: Image reconstruction, restoration, and alignment, with a focus in tomography." http://www.toby-sanders.com/software, https://doi.org/10.13140/RG.2.2.33492.60801.
[18] Ghiglia, D. C. and Pritt, M. D., [*Two-dimensional phase unwrapping: theory, algorithms, and software*], vol. 4, Wiley New York (1998).
[19] Goldstein, R. M., Zebker, H. A., and Werner, C. L., "Satellite radar interferometry: Two-dimensional phase unwrapping," *Radio science* **23**(4), 713–720 (1988).
[20] Fessler, J. and Sutton, B., "Nonuniform fast Fourier transforms using min-max interpolation," *IEEE Transactions on Signal Processing* **51**(2), 560–574 (2003).